On numerical errors in the boundary conditions of the Euler equations

Lars Ferm
Per Lötstedt

Technical report 2000-007
April 2000
ISSN 1404-3203

Department of Information Technology
Uppsala University

On numerical errors in the boundary conditions of the Euler equations

Lars Ferm and Per Lötstedt*

March 30, 2000

Abstract

Numerical errors in solution of the Euler equations of fluid flow are studied. The error equations are solved to analyze the propagation of the discretization errors. In particular, the errors caused by the boundary conditions and their propagation are investigated. Errors generated at a wall are transported differently in subsonic and supersonic flow. Accuracy may be lost due to the accumulation of errors along walls. This can be avoided by increasing the accuracy of the boundary conditions. Large errors may still arise locally at the leading edge of a wing profile. There, a fine grid is the best way to reduce the error.

Subject classification: 65N12

Keywords: Euler equations, solid wall, boundary conditions, error equations, error propagation

1 Introduction

A common difficulty when solving flow problems computationally is the choice and discretization of boundary conditions. The boundary values of the the analytical solution may not be self-evident and the numerical discretization often needs additional conditions at the true or artificial boundaries. These matters are discussed in [1] and [2].

There are different sources of numerical error at a boundary. One part is due to the grid spacing h and another part is caused by approximations e.g. at an outflow or outer open boundary. While the first error is controlled by h, the latter usually decreases independent of h as the distance from the boundary increases. The approximation of boundary conditions is treated e.g. in [3], [4], [5].

The purpose of this note is to show how boundary errors are created and propagate in the solution of the steady, incompressible and compressible Euler equations. We demonstrate striking improvements of accuracy obtained by increasing the order of the boundary conditions, but we also give en example where high order conditions must be used with care.

*Dept. of Information Technology, Scientific Computing, Uppsala University, SE-75104 Uppsala, Sweden

The accumulation of errors generated by the discretization is treated in Sect. 2. Equations are derived for the errors in the solution, in particular the influence of the boundary in a finite volume discretization is studied. In 2D, the solution errors due to discretization errors at the boundaries decay away from the boundary in subsonic flow. In supersonic flow the errors are advected without attenuation. At boundaries without a parallel streamline (or more generally, without a parallel characteristic) we may use boundary conditions of order $\nu - 1$ and still get an error of order ν in the obtained solution [6]. This is not the case at solid walls.

In Sect. 3 we consider incompressible flow and extrapolation to determine numerical boundary conditions. A plot of the solution on and outside the leading edge of a wing profile may look smooth, but there are very large derivatives on the surface. We conclude that high order boundary conditions should be avoided here on coarser grids, including those of coarser multigrid levels. This problem does not appear in computations around a cylinder where there are no large derivatives.

We use body-fitted, structured grids in the numerical examples, but the analysis is applicable to other types of grids such as Cartesian grids and unstructured grids.

2 Error equations

The Euler equations are discretized by a finite volume method and the average $\bar{u}$ of the steady state solution u is computed in each cell. To solve

$$\nabla \cdot \mathcal{F}(u) = 0 \text{ in } \Omega, \tag{1}$$

for u with boundary conditions on $\partial\Omega$, (1) is first integrated over a cell ω_j with boundary $\partial\omega_j$ and area A_j

$$A_j^{-1} \int_{\omega_j} \nabla \cdot \mathcal{F}(u) d\omega = A_j^{-1} \int_{\partial\omega_j} \mathcal{F}(u) \cdot \hat{n} ds = F_j(u) = 0. \tag{2}$$

Let cell j have l straight edges and and let edge i have normal $\hat{n}_i$ and length Δs_i. Then with the discrete flux $\Psi_j^i(u)$, Φ_j in

$$\Phi_j(\bar{u}) = A_j^{-1} \sum_{i=1}^{l} \Psi_j^i(u) \cdot \hat{n}_i \Delta s_i \tag{3}$$

approximates F_j in (2). The cells $\omega_j,\ j = 1 \ldots N$, cover Ω.

Equations for the error in the numerical solution are derived in [7]. Let the analytical solution of (2) for all j be denoted by $\hat{u}$ and the numerical error by δu. The numerical solution reconstructed from the computed averages is $u = \hat{u} + \delta u$. If τ is the discretization error caused by the finite volume method, then we have for $w = u$ or $\hat{u}$

$$F_j(w) - \Phi_j(\bar{w}) = \tau_j(w). \tag{4}$$

When $w = \hat{u}$ then $\Phi_j(\bar{w}) = -\tau_j(w)$ and when $w = u$ then $F_j(w) = \tau_j(w)$.

For the Euler equations, let ρ be the density, $\mathbf{U} = (u, v)^T$ the velocity, p the pressure, and H the total enthalpy. Then the equations in conservation form satisfied by the numerical solution in 2D are [7]

$$(\rho u)_x + (\rho v)_y = \tau_1, \tag{5a}$$

$$(\rho u^2)_x + (\rho uv)_y + p_x = \tau_2, \tag{5b}$$

$$(\rho uv)_x + (\rho v^2)_y + p_y = \tau_3, \tag{5c}$$

$$(\rho uH)_x + (\rho vH)_y = \tau_4. \tag{5d}$$

The subscript x or y denotes derivation with respect to the independent variable. The analytical solution satisfies (5) with $\tau = 0$. The system is closed by the relations

$$q^2 = u^2 + v^2,\ \ H = \gamma p/((\gamma - 1)\rho) + q^2/2,$$

where γ is the gas constant. The entropy S of the flow is defined by

$$S = \log(p/\rho^\gamma). \tag{6}$$

The error equations for H and for a constant S become [7]

$$\delta H = \int \tau_H \, ds, \tag{7a}$$

$$\delta S = \int \tau_S \, ds, \tag{7b}$$

where s is the arc length along a stream line, and

$$\tau_H = (\tau_4 - H\tau_1)/(\rho q), \tag{8a}$$

$$\tau_S = \frac{\gamma - 1}{p}(q\tau_1 - \frac{u\tau_2 + v\tau_3}{q} + \rho\tau_H). \tag{8b}$$

In incompressible flow, we let $\rho = 1$ and ignore (5d). The error equation for the total pressure $P = p + (u^2 + v^2)/2$ is also integrated along a streamline

$$\delta P = \int \tau_P \, ds, \tag{9}$$

where $\tau_P = (u\tau_2 + v\tau_3)/q - q\tau_1$.

The errors in H and S in the compressible case, and in P in the incompressible case are thus integrated discretization errors along streamlines. For a cell j with one edge on a boundary, suppose that the error in the boundary condition is such that τ_j is of $\mathcal{O}(h^{\nu-1})$ and τ in the interior of Ω is of $\mathcal{O}(h^\nu)$. If a streamline follows a boundary, this means that δH, δS or δP in (7), (8), and (9) are of the same order in h as the boundary conditions. A lower order accuracy in H, S, or P will pollute the solution in $\rho, \mathbf{U}$ and p. At other types of boundaries, where no streamlines follow the boundary, we may use a boundary approximation introducing an error of order $\nu - 1$ at a finite number of points, independent of h, if the method used in the interior is of order ν. The error in the obtained solution will still be of order ν [6].

The error equations are particularly simple if we make the following assumptions:

1. All derivatives of the analytical solution are small,
2. u, ρ, and p are of $\mathcal{O}(1)$ but v is small,
3. The errors in the solution are small.

Then the errors satisfy [7]

$$\begin{aligned}
\hat{\rho}\nabla \cdot \delta\mathbf{U} + \hat{u}\delta\rho_x &= \tau_1, && \text{(10a)}\\
\hat{\rho}\hat{u}\delta u_x + \delta p_x &= \tau_2 - \hat{u}\tau_1 = \tau_2', && \text{(10b)}\\
\hat{\rho}\hat{u}\delta v_x + \delta p_y &= \tau_3, && \text{(10c)}\\
(1 - M^2)\delta p_{xx} + \delta p_{yy} &= (1 - M^2)\tau_{2x}' + \tau_{3y} - \hat{\rho}\hat{u}\tau_{4x}' = \tau_p, && \text{(10d)}
\end{aligned}$$

where

$$\tau_4' = -\hat{u}\tau_2'/\hat{p} + (\gamma - 1)(\tau_4 - 0.5\hat{u}^2\tau_1)/(\gamma\hat{p}),$$

and M denotes the Mach number with definition $M^2 = \rho(u^2 + v^2)/(\gamma p)$.

Let us consider the domain $\Omega = \{x \geq 0,\ y \geq 0\}$. For subsonic flow with $M < 1$, the error equation for the pressure in (10d) is rewritten with $\beta^2 = 1 - M^2$ and the coordinate transformation $x' = x/\beta$. Then

$$\begin{aligned}
&\delta p_{x'x'} + \delta p_{yy} = \nabla \cdot \tau' \text{ in } \Omega,\\
&\delta p(x', 0) = \delta p_0,\ \delta p(0, y) = \delta p_1,
\end{aligned} \tag{11}$$

since τ_p can be written as a divergence.

The Green's function of (10d) with $\delta p_0 = \delta p_1 = 0$ is [8], [9]

$$\begin{aligned}
g(x', y, \xi, \eta) = \quad & g_1(x' - \xi, y - \eta) - g_1(x' - \xi, y + \eta)\\
& -g_1(x' + \xi, y - \eta) + g_1(x' + \xi, y + \eta),\\
g_1(x, y) = \quad & \tfrac{1}{4\pi}\log(x^2 + y^2).
\end{aligned} \tag{12}$$

Then with homogeneous boundary conditions, the solution to (11) is by Gauss' theorem

$$\begin{aligned}
\delta p_h(x/\beta, y) = \quad & \int_\Omega \nabla \cdot \tau' g \, d\Omega =\\
& \int_{\partial\Omega} n \cdot \tau' g \, ds - \int_\Omega \tau' \cdot \nabla g \, d\Omega = -\int_\Omega \tau' \cdot \nabla g \, d\Omega,
\end{aligned} \tag{13}$$

since $g = 0$ on $\partial\Omega$. The solution to (11) with $\tau' = 0$ is

$$\delta p_b(x/\beta, y) = \int_{\partial\Omega} n \cdot \nabla g \, \delta p \, ds. \tag{14}$$

By superposition, the solution to (11) is

$$\delta p(x/\beta, y) = \delta p_h + \delta p_b = \int_{\partial\Omega} n \cdot \nabla g \, \delta p(\xi, \eta) ds - \int_{\Omega} \tau'(\xi, \eta) \cdot \nabla g \, d\Omega. \tag{15}$$

Since

$$\nabla g_1(x', y) = \frac{\mathbf{r}}{2\pi r^2}, \ \mathbf{r} = (x', y)^T, \ r = |\mathbf{r}|,$$

the influence of a discretization error τ' at (ξ, η) and an error δp in the boundary condition at $(\xi, 0)$ or $(0, \eta)$ decays as $1/r$, where r is the distance to (x, y).

For supersonic flow $M > 1$ let $\beta^2 = M^2 - 1$ and use the same transformation as in (11). Then in regions without discontinuities such as shocks we have

$$\begin{aligned} &\delta p_{x'x'} - \delta p_{yy} = -\tau_p \text{ in } \Omega, \\ &\delta p(x', 0) = \delta p_0, \ \delta p_{x'}(0, y) = \delta p_{x1}/\beta, \ \delta p(0, y) = \delta p_1. \end{aligned} \tag{16}$$

Let $H(x)$ and $\delta(x)$ denote the Heaviside and Dirac functions. The Green's function of (16) with $\delta p_0 = 0$ is [9] (cf. Fig.1)

$$g(x', y, \xi, \eta) = 0.5(H(x' - \xi - |y - \eta|) - H(x' - \xi - |y + \eta|)). \tag{17}$$

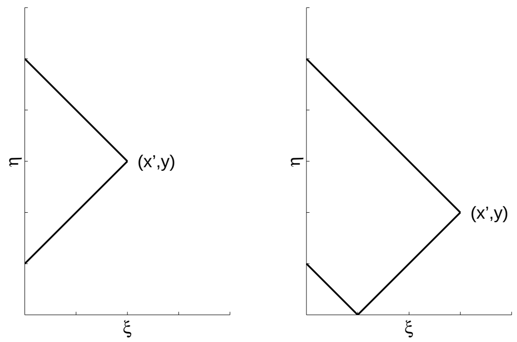

Figure 1: The support of the Green's function g in (17) when $y > x'$ (left) and $x' > y$ (right).

The solution to (16) with $\delta p_0 = 0$ can now be written

$$\delta p_h(x/\beta, y) = -\int_\Omega \tau_p g \, d\Omega + \int_0^\infty \delta p_{x1}(\eta) g/\beta \, d\eta + \tfrac{d}{dx'} \int_0^\infty \delta p_1(\eta) g \, d\eta. \tag{18}$$

In the first integral in (18), τ_p is integrated over the domain where g in (17) has support in $[0, \infty] \times [0, \infty]$, see Fig. 1. The second integral in (18) is

$$I_2 = \begin{cases} 0.5\beta^{-1} \int_{y-x'}^{y+x'} \delta p_{x1}(\eta) d\eta, & y \geq x', \\ 0.5\beta^{-1} \int_{x'-y}^{y+x'} \delta p_{x1}(\eta) d\eta, & x' > y. \end{cases} \tag{19}$$

The third integral is

$$\frac{d}{dx'}I_3 = \begin{cases} 0.5(\delta p_1(y-x') + \delta p_1(y+x')), & y \geq x', \\ 0.5(\delta p_1(y+x') - \delta p_1(x'-y)), & x' > y. \end{cases} \tag{20}$$

The solution to (16) with $\delta p_1 = \delta p_{x1} = 0$ is

$$\delta p_b(x/\beta, y) = \begin{cases} 0, & y \geq x', \\ \delta p_0(x'-y), & x' > y. \end{cases} \tag{21}$$

Since

$$\delta p(x/\beta, y) = \delta p_h(x', y) + \delta p_b(x', y),$$

it follows from (18), (19), (20), and (21) that the discretization errors and the errors in the boundary conditions are propagated into Ω from the boundary without damping in the supersonic case in 2D.

From (10b) we conclude that

$$\delta u(x,y) = (\hat{\rho}\hat{u}(0,y)\delta u(0,y) + \int_0^x \tau_2'(\xi, y)d\xi + \delta p(0,y) - \delta p(x,y))/(\hat{\rho}\hat{u}). \tag{22}$$

If the boundary error $\delta u(0,y)$ is of $\mathcal{O}(h^\nu)$, then the error in the flux function Ψ in (3) at $x=0$ is of $\mathcal{O}(h^\nu)$. Hence, $\tau_2' = \mathcal{O}(h^{\nu-1})$ in the first cell column. If $\tau_2' = \mathcal{O}(h^\nu)$ in the interior and $\delta p(x,y)$ is of order ν, then $\delta u(x,y)$ is also of order ν. A similar equation is satisfied by $\delta\rho$ [7]. It is also shown in [7] that δv fulfills the same equations as δp in (11) and (16) with a different right hand side.

Incompressible flow along a curved boundary is best investigated in polar coordinates (r, θ). Let U and V denote the velocity components in the circumferential and the radial directions, respectively. Then the error equations are

$$V_r + U_\theta/r + V/r = \tau_1, \tag{23a}$$

$$VV_r + UV_\theta/r - U^2/r + p_r = \tau_2, \tag{23b}$$

$$VU_r + UU_\theta/r + UV/r + p_\theta/r = \tau_3. \tag{23c}$$

The analytical solution $(\hat{U}, \hat{V}, \hat{p})$ satisfies (23) with $\tau_j = 0,\ j = 1,2,3.$ Assume that

1. $\hat{V}$, $\hat{V}_\theta$, and V_θ are small
2. The errors in the solution are small and $\delta V \ll \delta p, \delta U$.

The first assumption is valid close to a cylindrical surface where $r = a$ and $\hat{V} = 0$. After dropping quadratic terms in the errors and using the assumptions, the errors in p and U satisfy

$$\delta p_r - 2(U\delta U)/r = \tau_2, \tag{24a}$$

$$\delta p_\theta + (U\delta U)_\theta = r\tau_3. \tag{24b}$$

Take the θ-derivative of (24a), the r-derivative of (24b) and rewrite (24) to obtain

$$\begin{array}{ll} \delta p_{r\theta} + \frac{2}{r}\delta p_{\theta} & = \tau_{2\theta} + 2\tau_3, \\ (U\delta U)_{r\theta} + \frac{2}{r}\delta (U\delta U)_{\theta} & = (r\tau_3)_r - \tau_{2\theta}. \end{array} \tag{25}$$

Let

$$\begin{array}{ll} \sigma_2(r,\theta) & = c_2 + \tau_2 + 2\int_0^{\theta} \tau_3 d\phi, \\ \sigma_3(r,\theta) & = c_3 - \tau_2 + r\int_0^{\theta} \tau_{3r} d\phi, \end{array} \tag{26}$$

where c_2 and c_3 are integration constants determined by the boundary conditions at $\theta = 0$. Then the solution to (25) is

$$\begin{array}{l} \delta p(r,\theta) = (\int_a^r \rho^2\sigma_2 d\rho + a^2\delta p(a,\theta))/r^2, \\ U\delta U(r,\theta) = (\int_a^r \rho^2\sigma_3 d\rho + a^2 U\delta U(a,\theta))/r^2. \end{array} \tag{27}$$

If the discretization error is concentrated at the boundary, e.g. on a cylinder with radius a $\tau_2, \tau_3 \approx 0$, when $r > a$, and in the boundary conditions, then δp and δU decay as $1/r^2$ for growing r. The error τ_3 in the streamline direction in (23c) and (24b) is accumulated along the boundary in σ_2 and σ_3 in (26).

The conclusions in this section are valid for finite difference, finite element, and finite volume methods.

3 Numerical boundary conditions

The steady state solution of the Euler equations of incompressible flow are computed with different numerical boundary conditions at solid walls in this section. The computational domain Ω is covered by a structured grid and the equations are approximated by the method of Jameson, Schmidt, and Turkel [10]. The artificial viscosity in the scheme is computed as a fourth difference of the variables divided by the grid size. Ghost cells are added outside Ω to simplify the treatment at the boundaries. The values of the dependent variables there are given by the numerical boundary conditions.

The velocity components in the ghost cells at a solid wall are determined such that if the normal velocity is $\mathbf{U} \cdot n$ in the interior cell at the surface, then it is $-\mathbf{U} \cdot n$ in the ghost cell. Extrapolation from the interior provides values for the tangential velocity component, ρ, and p in the ghost cells.

When extrapolating p in the normal direction from the closest interior cell 1 to the ghost cell 0 we make the following approximation

$$p_0 = p_1 + hp_n + h^2 p_{nn}/2 + h^3 p_{nnn}/6 + h^4 p_{nnnn}/24 + \dots \tag{28}$$

where n denotes differentiation in the normal direction to the surface. With ν:th order extrapolation, i.e. the ν:th order difference vanishes, the error in p_0 in (28) and δp on the boundary are proportional to $h^\nu \partial^\nu p/\partial n^\nu$. Therefore, the error in the flux Ψ on the boundary will be of $\mathcal{O}(h^\nu)$ and τ in the cell there of $\mathcal{O}(h^{\nu-1})$. The effect of the artificial viscosity on τ is the same. With second order extrapolation we have first order discretization errors and an oscillatory behavior of the artificial viscosity at the boundary.

If there is no vorticity in the Euler solution, then it is equal to the linearized potential flow solution with a potential Φ satisfying

$$\begin{array}{l} \Delta\Phi = 0 \text{ in } \Omega,\ \mathbf{U} = \nabla\Phi,\ P = p + 0.5q^2 = \text{const}, \\ \mathbf{U} = (1,0)^T \text{ at } \infty, n\cdot\mathbf{U} = 0 \text{ on the surface.} \end{array} \tag{29}$$

For certain geometries in 2D, the analytical solution of (29) is available, e.g. the flow around a cylinder. Assuming vortex-free flow, the numerical solution of the Euler equations is compared to the analytical potential flow solution for two geometries: a cylinder and a Karman-Trefftz airfoil. The transformation

$$\left\{ \begin{array}{lcl} \zeta &=& (1-\zeta_0)z + \zeta_0 \\ w &=& k\frac{(\zeta+1)^k + (\zeta-1)^k}{(\zeta+1)^k - (\zeta-1)^k},\ k = (2\pi - \theta)/\pi, \end{array} \right. \tag{30}$$

maps the unit circle $z = 1$ onto the Karman-Trefftz profile in the w-plane and also the analytical solution from the exterior of the cylinder to the exterior of the airfoil. In these examples, the variables at the outer open boundary are determined by the potential solution.

In a third example, the flow in a channel is computed. The numerical results for the cylinder, airfoil, and channel agree very well with the expected order of accuracy and the error propagation properties in Sect. 2.

3.1 Cylinder

The flow around a cylinder of radius 2 is computed with the boundary data in (29). The discretization errors τ in (5) are calculated by inserting the analytical solution into the discretization. The dominant part in τ_P in (9) is found at the boundary, see Fig. 2. Fourth order extrapolation perturbs the $\mathcal{O}(h^2)$ error of the method in the interior by only $\mathcal{O}(h^3)$.

The errors in the total pressure P along one side of the cylinder are plotted in Fig.3 for second and fourth order extrapolations in the cells along the cylinder surface. Each figure contains results from two different grids of size 32×16 and 64×32. The Figs. 2 and 3 confirm the error behavior in (27) and the predicted orders of accuracy.

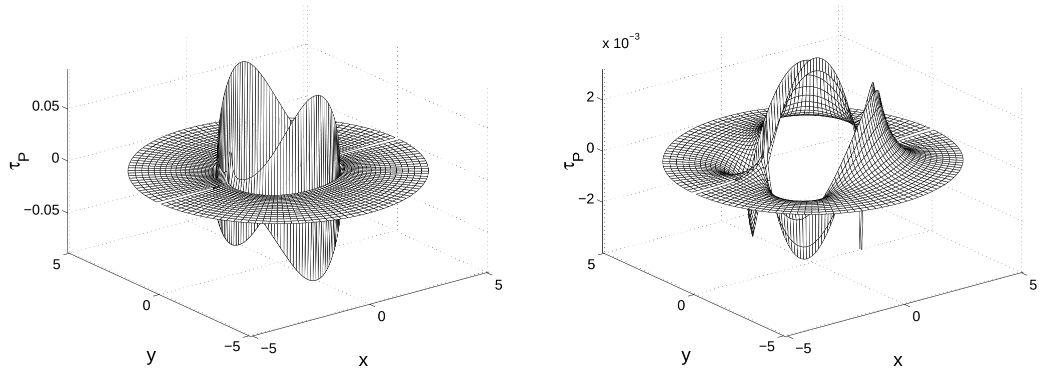

Figure 2: Discretization error around a cylinder for second (left) and fourth (right) order extrapolation in the ghost cells.

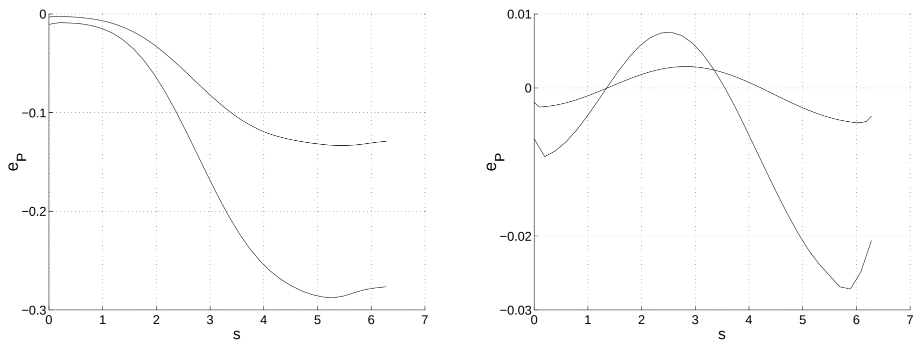

Figure 3: The effect on δP of doubling the grid size using second (left) and fourth (right) order of extrapolation into the ghost cells.

3.2 Karman-Trefftz profile

We choose the parameters $\zeta_0 = -1,\ \theta = 10$ in our example to obtain the geometry in Fig. 4.a.

While higher order extrapolation yields satisfactory results for the cylinder, this is not necessarily so for the airfoil. The derivatives of p in the normal direction at the leading edge are computed in Table 1 for the wing profile and a cylinder.

Table 1: Normal derivatives at the leading edge.

	wing	cylinder
p	2.5	2.5
p_n	0	0
p_{nn}	$-2.76 \cdot 10^2$	-4
p_{nnn}	$-3.35 \cdot 10^4$	-36
p_{nnnn}	$-4.35 \cdot 10^6$	-300

The higher derivatives of the wing profile are much larger than the corresponding ones at the cylinder. Extrapolations approximate the analytic continuation by assuming a higher order difference in the normal direction to be 0 in (28). The table indicates that values from (28) are useless as boundary data on coarser grids at the leading edge of the airfoil.

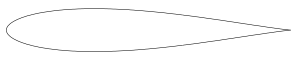

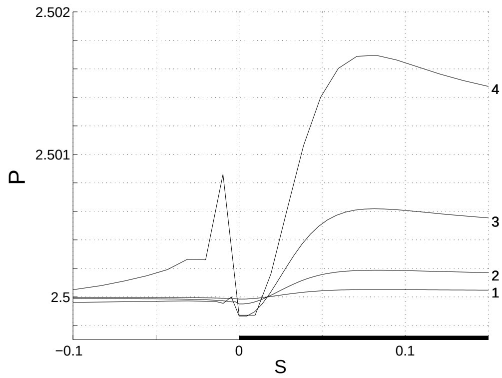

a b

Figure 4: (a) The Karman-Trefftz profile. (b) Total pressure P in front of the wing profile ($s < 0$) continued along the surface of the profile ($s > 0$).

Numerical solutions at the leading edge of the Karman-Trefftz profile are plotted Fig. 4.b. The total pressure is displayed along the symmetry line ($s < 0$) and along a part of the surface ($s > 0$). The grid size is doubled three times when going from 1 to 4. Grid 4 is already a relatively fine grid with h equal to about 1/750 of the chord length. Yet we have to refine this grid to avoid the error peak at the leading edge.

3.3 Channel

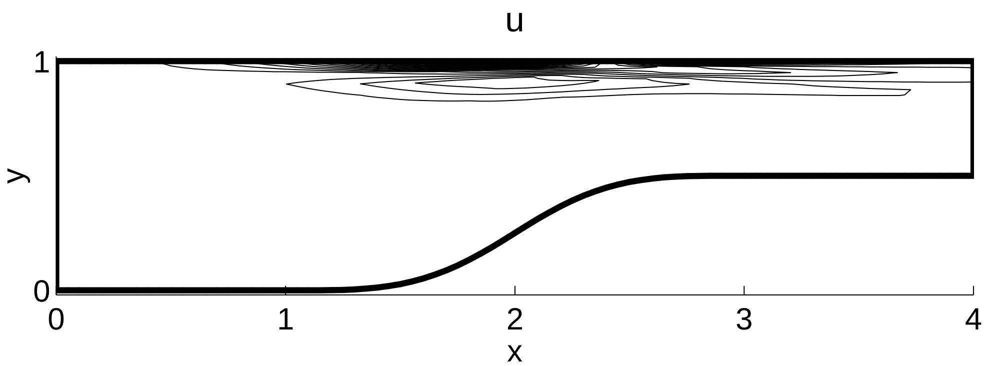

Figure 5: Difference in u generated by different extrapolations at the boundary.

The channel in Fig. 5 has solid upper and lower walls. The direction of the flow is from left to right. The solution to the Euler equations is computed with second and fourth order extrapolation at the upper wall. The solutions are subtracted from each other and the isolines of the difference in u are shown.

The difference in the solution is generated by a different τ in (5) at the boundary in the contraction of the channel. This difference is localized close to the boundary and is transported downstream according to (22).

Acknowledgment

Financial support has been obtained from the Swedish Research Council for Engineering Science.

References

[1] W. L. Oberkampf, F. G. Blottner, Issues in computational fluid dynamics code verification and validation, *AIAA J.*, 36 (1998), p. 687–695.

[2] P. Roache, Quantification of uncertainty in computational fluid dynamics, *Annu. Rev. Fluid Mech.*, 29 (1997), p. 123–160.

[3] A. Dadone, B. Grossman, Surface boundary conditions for the numerical solution of the Euler equations, *AIAA J.*, 32 (1994), p. 285–293.

[4] C. Hirsch, *Numerical Computation of Internal and External Flows*, Vol. 2, Wiley, Chichester, 1990.

[5] A. Rizzi, Numerical implementation of solid boundary conditions for the Euler Equations, *ZAMM*, 58 (1978), p. T301–T304.

[6] B. Gustafsson, The convergence rate for difference approximations to mixed initial boundary value problems, *Math. Comput.*, 29 (1975), p. 396–406.

[7] L. Ferm, P. Lötstedt, Adaptive error control for steady state solutions of inviscid flow, Report 2000-003, Dept. of Information Technology, Uppsala University, Uppsala, Sweden, 2000.

[8] M. Renardy, R. C. Rogers, *An Introduction to Partial Differential Equations*, Springer-Verlag, New York, 1993.

[9] I. Stakgold, *Green's Functions and Boundary Value Problems*, Wiley, New York, 1998.

[10] A. Jameson, W. Schmidt, E. Turkel, Numerical solutions of the Euler equations by finite volume methods using Runge-Kutta time-stepping schemes, AIAA-paper 81-1259, 1981.